



UvA-DARE (Digital Academic Repository)

Structured doping of upconversion nanosystems for biological applications

Wang, Y.

Publication date
2011

[Link to publication](#)

Citation for published version (APA):

Wang, Y. (2011). *Structured doping of upconversion nanosystems for biological applications*. [Thesis, fully internal, Universiteit van Amsterdam].

General rights

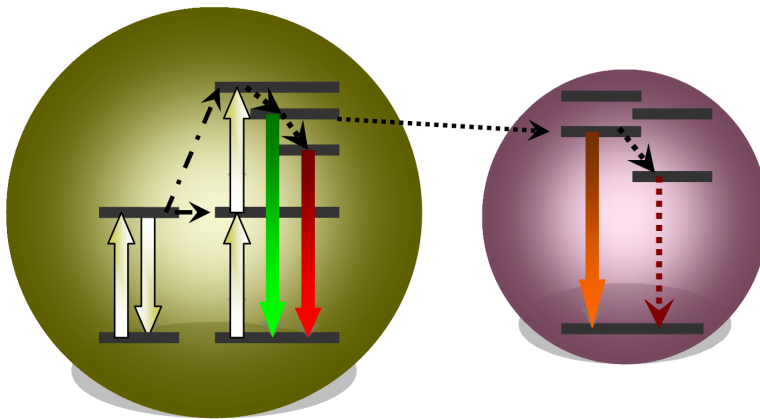
It is not permitted to download or to forward/distribute the text or part of it without the consent of the author(s) and/or copyright holder(s), other than for strictly personal, individual use, unless the work is under an open content license (like Creative Commons).

Disclaimer/Complaints regulations

If you believe that digital publication of certain material infringes any of your rights or (privacy) interests, please let the Library know, stating your reasons. In case of a legitimate complaint, the Library will make the material inaccessible and/or remove it from the website. Please Ask the Library: <https://uba.uva.nl/en/contact>, or a letter to: Library of the University of Amsterdam, Secretariat, P.O. Box 19185, 1000 GD Amsterdam, The Netherlands. You will be contacted as soon as possible.

CHAPTER 6

Critical Shell Thickness of Core/shell Upconversion Luminescence Nanoplatforms for FRET Applications



Chapter 6

Abstract: The influence of the structure of upconversion nanoparticles on their fluorescence resonant energy transfer applications has been studied using core/shell upconversion $\text{NaYF}_4:\text{Yb}^{3+},\text{Er}^{3+}@\text{NaYF}_4$ nanoparticles and rose bengal photosensitizer. From studies of the photophysics of and singlet oxygen generation by the conjugates of upconversion nanoparticles with photosensitizers we have determined what the optimal shell thickness is for the performance of the FRET conjugates. It has been found that the optimal shell thickness is a trade-off between the opposing optimal conditions for upconversion and FRET efficiency.

Keywords: upconversion · nanoparticle · core/shell · photosensitizer · energy transfer efficiency · singlet oxygen · photodynamic therapy

6.1 Introduction

Rare earth ions (RE^{3+}) doped upconversion nanoparticles (UCNPs) have recently been introduced as energy donor for Förster resonant energy transfer (FRET) based applications in biological/biomedical fields.^[1] FRET is a direct and effective method widely used in bioassays,^[2] biosensing and bioimaging^[3], and photodynamic therapy.^[4] In comparison to traditional fluorescent energy donors such as organic dyes and quantum dots, the advantages of UCNPs derive from their unique property of being able to emit multicolor visible light under continuous wave NIR light. Due to the absence of autofluorescence and reduction of light scattering under such conditions an excellent signal-to-noise ratio in detection can be obtained. From a biomedical point of view, the use of NIR light is very attractive, since NIR radiation has a higher tissue penetration than normal UV-Vis radiation and leads to less photodamage to living organisms. There is thus a large area of bio-applications where such systems could potentially significantly advance the state-of-the-art.

However, as yet the poor upconversion efficiency of UCNPs with an upper limit of only a few percent has been a serious hurdle. This is certainly true for biological applications where excitation power is restricted and the upconversion efficiency is thus even an order of magnitude lower. In recent years large efforts have been devoted to improve the upconversion intensity of UCNPs. One strategy is to use a core/shell structure (such as $\text{NaYF}_4:\text{RE}^{3+}@\text{NaYF}_4$) where a shell of the same or similar material as the core is grown on the surface of the core.^[5] This strategy aims to protect the excited activators - emitters, such as Er^{3+} , Tm^{3+} ions in the core, especially those near the surface - from non-radiative loss caused by surface defects and high-energy vibrational modes outside the particle. Our previous work^[5f,5g] has demonstrated already that a large enhancement of the upconversion emission intensity can be achieved by such a core/shell structure.

However, a high upconversion yield does not guarantee high-quality performance in afore-mentioned FRET applications, because the energy transfer efficiency from donor to acceptor could be impaired in the effort of enhancing upconversion luminescence. As is well known, FRET is a nonradiative process where an excited state donor transfers its energy to a proximal ground state acceptor. The rate of energy transfer strongly depends on the distance between the donor and the acceptor. As far as the core/shell approach is concerned, a thick shell favors usually the upconversion luminescence within the saturation limit, whereas the distance between the donor, (basically the core where emitters are located) and the acceptor (usually the organic molecules on the surface of the nanoparticle) is becoming larger when the shell is getting thicker. Therefore, for FRET application the shell of the core/shell UCNPs can not be increased to such an extent that the strongest upconversion luminescence is reached.

Chapter 6

In this work core/shell structured $\text{NaYF}_4:\text{RE}^{3+}@\text{NaYF}_4$ UCNPs are introduced for the first time together with photosensitizing molecules to form a FRET model for PDT application. The relationship between the shell thickness and $^1\text{O}_2$ generation is studied in detail. The most important result is that there is an optimal value for the shell thickness, which corresponds neither to the thickness for which the strongest upconversion luminescence is reached nor to the thickness for which the highest energy transfer efficiency is obtained.

6.2 Experiments

6.2.1 Chemicals

$(\text{CF}_3\text{COO})_3\text{Y}\cdot 3\text{H}_2\text{O}$, $(\text{CF}_3\text{COO})_3\text{Yb}\cdot 3\text{H}_2\text{O}$ and $(\text{CF}_3\text{COO})_3\text{Er}\cdot 3\text{H}_2\text{O}$ were purchased from *GFS Chemicals*, CF_3COONa , oleylamine (OM), rose bengal (RB), 6-bromohexanoic acid, poly(allylamine) (PAAm) solution (Mw~17000), 1-ethyl-3-(3-dimethylaminopropyl) carbodiimide (EDC), and N-hydroxy succinimide (NHS) were purchased from *Aldrich*. 1,3-diphenylisobenzofuran (DPBF) was purchased from *Fluka*. Ethanol and hexane were of analytical grade.

6.2.2 Synthesis of $\text{NaYF}_4:\text{Yb}^{3+},\text{Er}^{3+}@\text{NaYF}_4$ core/shell structured upconversion nanoparticle

The synthesis of $\text{NaYF}_4:\text{Yb}^{3+},\text{Er}^{3+}@\text{NaYF}_4$ core/shell structured upconversion nanoparticles has been performed similar to the procedures reported previously.^[4g, 6] Briefly, a mixture of designated molar ratio of trifluoroacetate salts powder ($\text{Na}^+/\text{RE}^{3+} = 1/1$, $\text{Y}^{3+}/\text{Yb}^{3+}/\text{Er}^{3+} = 78/20/2$ mol/mol) was dissolved in oleylamine (OM) and then passed through a filter to get rid of the residues. Under vigorous stirring in a three neck flask, the mixture was heated to 110 °C under vacuum and maintained at this temperature to remove the residual water and oxygen for more than 30 min. During this time the flask was purged periodically with dry argon gas for protection from oxidation. Afterwards the solution was clear with a slight orange color. The mixture was subsequently slowly heated to 310 °C in the presence of an argon atmosphere. After half an hour, all the products were left to cool to room temperature and separated into six equal parts. Every part of the product we obtained was reheated to 310 °C under vigorous stirring and in a dry argon gas atmosphere, after which different amounts of shell precursors solutions containing sodium trifluoroacetate and yttrium trifluoroacetate of equal molarity were slowly added into the reaction systems. All the reactions that followed were allowed to continue for another half an hour. Every final mixture was left to cool to room temperature, precipitated with ethanol, and separated via centrifugation for at least three times. The resulting nanoparticles were dried in vacuum at 60 °C for a minimum of 24 hours. According to the increasing amount of shell materials we denote the samples as **A**, **B**, **C**, **D**, **E** and **F**.

6.2.3 Phase transfer of upconversion nanoparticle from hydrophobic to hydrophilic

A ligand exchange process was carried out to transfer hydrophobic upconversion nanoparticles to hydrophilic. 40 μL of poly(allylamine) (PAAm) solution (10% wt. in water) was dispersed in 10 ml ethanol, then 1 ml hydrophobic UCNPs solution (0.1 mmol/mL) was added drop by drop to the PAAm solution and stirred vigorously over 36 hours at 40 °C. After centrifugation (13000 rpm, 4 °C, 2 hours) the nanoparticles that were obtained were redispersed in water. In the resulting system, PAAm has replaced oleylamine as a ligand. The PAAm terminated UCNPs provide a terminal amino which can be used for covalently coupling with carboxyl terminated molecules.

6.2.4 Conjugation of upconversion nanoparticles and rose bengal photosensitizer

First, the RB-NHS ester was synthesized as a previous protocol.^[7] In the present work we want to compare singlet oxygen generation from the different UCNP-RB nanosystems and thus it was necessary to have the same ratio of RB/UCNP for all six samples. To this purpose, an ethanol solution of UCNPs with a concentration of 7.2×10^{13} particles/mL was mixed with 2.5 nmol RB-NHS at room temperature in the dark for 10 hours, leading to about 20 RB molecules attached on one nanoparticle. Almost all the RB molecules were bound covalently to the surface of UCNPs, and UCNP-RB conjugates were washed twice with water to remove the “free” photosensitizer.

6.2.5 Singlet oxygen measurements

Generation of $^1\text{O}_2$ by these UCNP- photosensitizers was detected chemically by 1,3-diphenylisobenzofuran (DPBF).^[8] Under reaction with singlet oxygen, DPBF is converted to its endoperoxide form, which in turn leads to its photobleaching. Bleaching was monitored by measuring the reduction in absorption intensity at 410 nm. To this purpose, 25 μL (2 mmol/L) DPBF solution was added to 1 ml ethanol solution of UCNPs with a concentration of 7.2×10^{13} particles/mL. The UV-Vis absorption spectrum of DPBF was measured every 5 minutes. The reduction in absorption was monitored as a function of time after irradiating samples with 980 nm diode laser. All measurements were performed at room temperature.

6.2.6 Characterizations

Structure characterization was performed with TEM images obtained with a MorgagniTM Transmission Electron Microscope (FEI Company). UV-Vis spectra of solutions were recorded in quartz cuvettes (1 cm) with a Hewlett-Packard/Agilent 8453 Diode-Array Biochemical Analysis UV-Vis Spectrophotometer. The steady-state upconversion spectrum of upconversion samples was measured with a SPEX Fluorolog 3 spectrometer using excitation from a CW semiconductor diode laser at 980 nm. The upconversion luminescence spectra were measured under identical conditions in order to compare their relative emission intensities. Time-resolved luminescence of upconversion

Chapter 6

samples was measured with a Hamamatsu R9110 PMT in a single-photon counting setup (Fast Comtec).^[9] For excitation a 980 nm laser pulse (~10 ns, 100 Hz) generated by a Nd:YAG laser system (Solar Inc.) was used.

6.3 Results and discussion

The core UCNP and five core/shell structured UCNP of different shell thicknesses were synthesized following a modified version of the well-known thermolysis method.^[6] A schematic illustration of the six samples is given in **Figure 6.1**. Sample **A** is the $\text{NaYF}_4:20\%\text{Yb}^{3+},2\%\text{Er}^{3+}$ core UCNP; samples **B**, **C**, **D**, **E** and **F** have the same core as **A** but a different shell thickness which was controlled during the synthesis. All of these six samples have good dispersibility in hexane. **Figure 6.1** shows the TEM images of the six hydrophobic samples. The average particle diameters are 16.0 nm (**A**), 20.2 nm (**B**), 23.0 nm (**C**), 27.4 nm (**D**), 34.4 nm (**E**) and 40.4 nm (**F**), corresponding to the shell thickness of 0 nm, 2.1 nm, 3.5 nm, 5.7 nm, 9.2 nm and 12.2 nm, respectively.

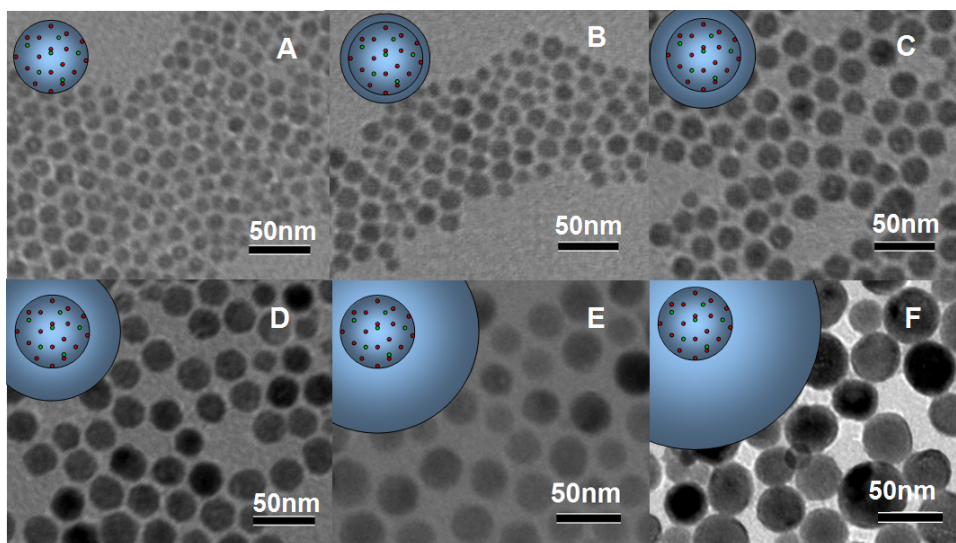


Figure 6.1. TEM results of six $\text{NaYF}_4: \text{Yb}, \text{Er}@ \text{NaYF}_4$ nanoparticles samples. Insets show a schematic illustration of the structures. **(A)**: $\text{NaYF}_4:20\%\text{Yb}^{3+},2\%\text{Er}^{3+}$ core UCNP. **(B)** to **(F)**: core/shell structure $\text{NaYF}_4:20\%\text{Yb}^{3+},2\%\text{Er}^{3+}@ \text{NaYF}_4$ UCNP with different shell thicknesses as described in the text.

The overlap of the RB absorption and UCNP emission spectra was shown in the previous chapter (**Figure 5.2 B**). These spectra show that energy transfer between RB and UCNP can occur. The mechanism of FRET from UCNP to RB photosensitizing

molecules upon 980 nm excitation is shown in **Figure 6.2**. Absorption of pump photons populates the $^2F_{5/2}$ level of Yb^{3+} , which is followed by energy transfer from excited Yb^{3+} ions to Er^{3+} ions, populating the $^4I_{11/2}$ level of the latter. Higher electronic levels of Er^{3+} , such as $^4F_{7/2}$ level, can then be populated by absorbing the energy of another excited Yb^{3+} ion or by direct absorption of another 980 nm photon. Part of the $^4I_{11/2}$ excited ions relaxes to the $^4I_{13/2}$ level through multiphonon non-radiative relaxation. The $^4F_{7/2}$ level can decay nonradiatively to the $^2H_{11/2}$, $^4S_{3/2}$ and $^4F_{9/2}$ levels, leading to the green emission bands around 520 and 540 nm, and the red emission band at 650 nm. Another population route of the $^4F_{9/2}$ level is by absorption of a 980 nm photon or energy transfer from another Yb^{3+} ion from the $^4I_{13/2}$ level of the Er^{3+} ions. The absorption band (520-570 nm) of RB overlaps well with the green emission band of UCNPs. Therefore, if RB molecules are bound to the surface of UCNPs, one should be able to excite them indirectly by 980 nm light via FRET through UCNPs.

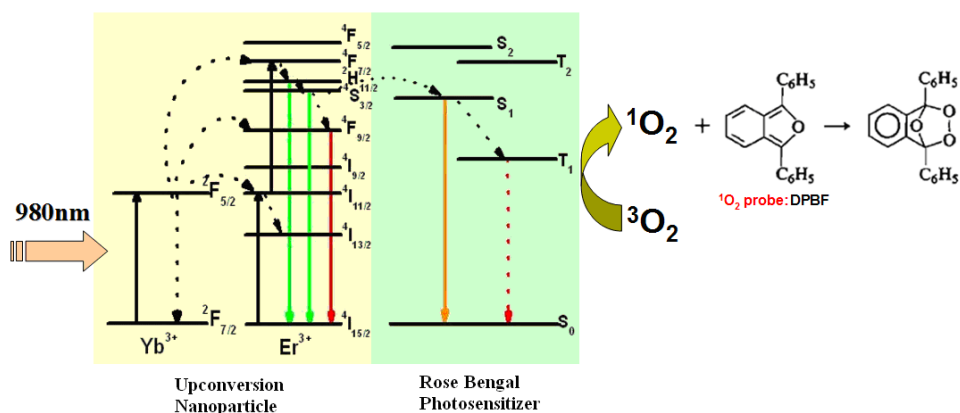


Figure 6.2. Mechanism of upconversion in the UCNP-RB nanoconjugate under excitation of 980 nm, and the oxidation reaction process of DPBF by 1O_2 .

The integrated intensities of the upconversion emission of the six samples are shown in **Figure 6.3 a**. This figure shows that the upconversion emission become monotonically stronger for thicker shells. We observe that upon binding with RB molecules the green upconversion emission decreases for all samples, consistent with the energy transfer from the upconversion nanoparticle to photosensitizing molecules. The energy transfer efficiency of this process can be calculated from the quenching value of donor luminescent intensity given by $E = (I_D - I_{DA}) / I_D$ where I_D and I_{DA} are emission intensities of the donor in the absence and presence of the acceptor, respectively.^[10] The result is shown in **Figure 6.3 b**. It is clear that for the bare core sample A-RB, 53% green emission is quenched, which is in line with the fact that the upconversion emission centers (donors) and photosensitizer molecules (acceptors) are very close leading to efficient

Chapter 6

energy transfer. For the core/shell structured upconversion samples the efficiency decreases monotonically from around 40% for sample **B** to less than 18% for sample **F**.

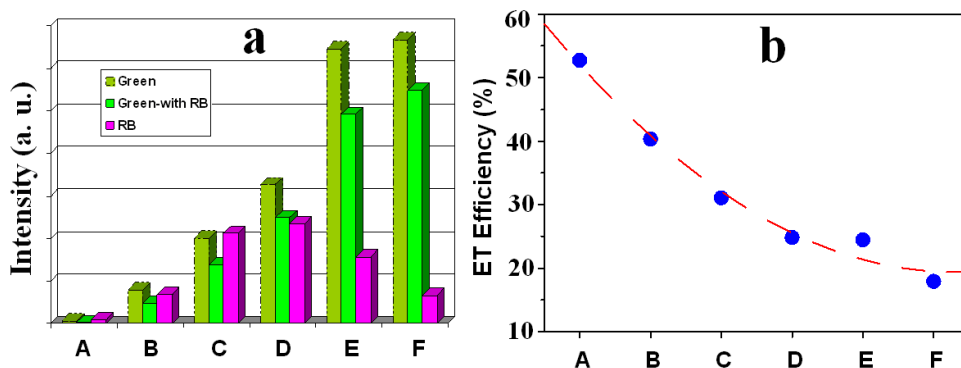


Figure 6.3. (a) Green upconversion emission intensity of samples **A-F** before (darker green columns) and after (green columns) RB attachment. Pink columns refer to the emission (580 nm) from RB, bound covalently to UCNPs. Excitation occurs by a CW diode laser at 980 nm with an excitation power of about 730 mW. (b) Energy transfer efficiency of the six UCNP-RB samples.

However, singlet oxygen generation does not only depend on the energy transfer efficiency. To study this in more detail we have monitored the fluorescence of RB in these samples (**Figure 6.3 a**). As illustrated in **Figure 6.2**, the fluorescence of RB can be used to measure the efficiency of RB excitation, provided that $S_1 \rightarrow T_1$ intersystem crossing is about the same in the six samples. The results shown in **Figure 6.3** demonstrate unambiguously that there exists an optimal shell thickness as far as the RB excitation is concerned. The samples **C**, **D** and **E** are in this respect the best with sample **D** showing the maximum emission. This means that a thinner or thicker shell is not efficient for exciting RB, even though a thin shell would favor energy transfer from nanoparticles to photosensitizer. This “inconsistency” actually reflects the surface dependence of the photophysics of upconversion nanoparticles. This is a typical feature of nanomaterials for which the surface is much more critical in determining their properties than for their bulk counterparts. In the present case the upconversion efficiency was enhanced with the increase of the shell thickness due to the better separation between the emitters in the core and the quenchers on the surface. The shell thickness therefore has two opposite effects on the excitation of RB. On the one hand, a thick shell facilitates a strong upconversion emission, and thus favors excitation of RB. On the other hand, a thick shell is not favourable for the energy transfer efficiency, and thus excitation of RB will be reduced. Combination of these two opposing effects thus indeed is expected to lead to an optimum in the fluorescence of RB as a function of the shell thickness.

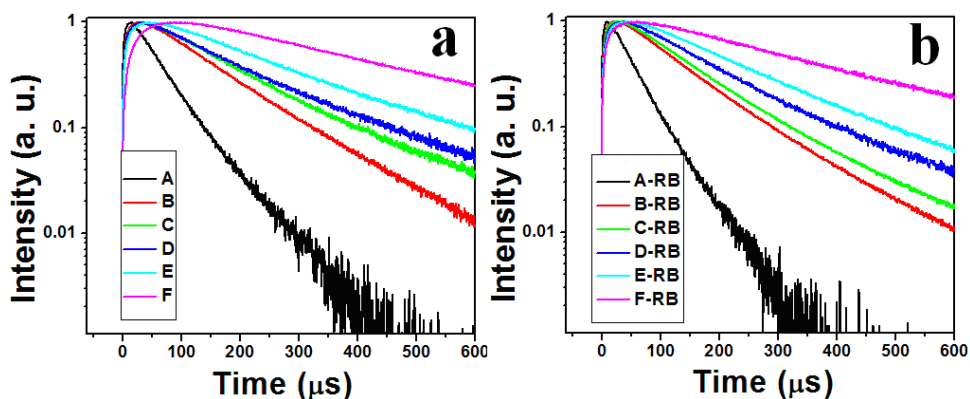


Figure 6.4. Temporal behavior of the 540 nm upconversion luminescence of the series of (a) UCNPs; (b) UCNP-RB conjugates. ($\lambda_{ex} = 980 \text{ nm}$)

To verify that RB was indeed excited by NIR light via energy transfer from UCNPs in this covalently bound nanoparticle-photosensitizer conjugate, we have determined the temporal behavior of the emission from these samples. **Figure 6.4** shows the time evolution of the 540 nm upconversion luminescence of the six UCNPs and the six UCNP-RB conjugates. Biexponential fits of the 540 nm emission decay lead to decay times listed in **Table 6.1**. From this Table it can be seen that the decay times of 540 nm emission of UCNP-RB conjugates are shorter than those of corresponding UCNPs.

Table 6.1. Results of fits of the 540 nm upconversion luminescence decay of the series of UCNPs and UCNP-RB conjugates.

	A	B	C	D	E	F
540 nm-rise (μs)	5.3	10.8	10.9	13.0	17.4	35.5
540 nm-decay (μs)	51.7	123.5	144.9	169.2	210.5	339.1
	A-RB	B-RB	C-RB	D-RB	E-RB	F-RB
540 nm-rise (μs)	4.1	8.4	8.5	9.9	16.2	19.1
540 nm-decay (μs)	42.7	109.4	119.9	154.5	184.4	312.3

The fluorescence lifetime of RB is of the order of tens of picoseconds,^[11] while the upconversion luminescence of Er^{3+} lasts much longer, usually (sub)microseconds. If RB is excited via energy transfer from UCNPs in the UCNP-RB conjugate, then the fluorescence of RB should be lengthened to the (sub)microsecond time scale. **Figure 6.5** records the temporal behavior of the RB fluorescence at 580 nm for the six UCNP-RB conjugates, and demonstrates that indeed all the decays are extended to the microsecond

Chapter 6

regime. **Figure 6.5** shows that the thicker the shell (from **A** to **F**), the longer the trace, exactly the same as observed for the temporal behavior of upconversion luminescence of UCNPs. Fits of the emission traces in **Figure 6.5** to a biexponential function are given in **Table 6.2**. From this Table it is clear that the microsecond rise component as well as the even longer decay component increase with the shell thickness. Thus time-resolved fluorescence confirms that FRET occurs in UCNP-RB conjugates.

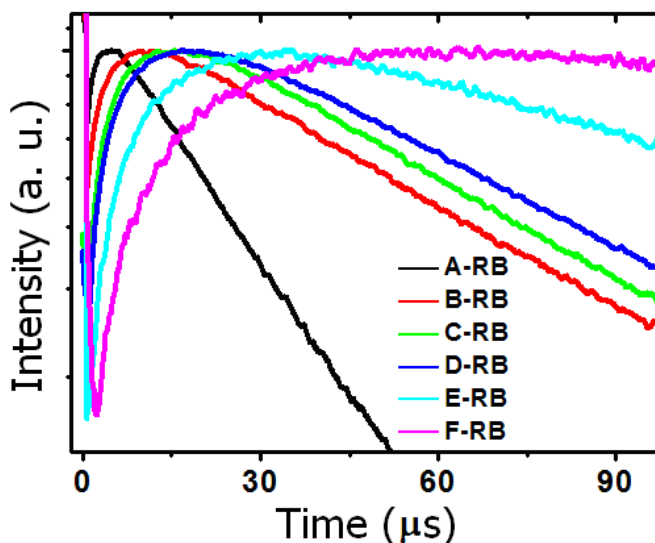


Figure 6.5. Temporal behavior of the 580 nm emission from the six UCNP-RB samples A-F after excitation at 980 nm.

Table 6.2. Fitting results of 580 nm emission of the six UCNP-RB samples.

	A-RB	B-RB	C-RB	D-RB	E-RB	F-RB
580 nm-rise (μs)	1.9	3.8	5.8	7.3	12.4	23.1
580 nm-decay (μs)	24.2	65.7	68.7	72.1	124.6	258.2

The generation of singlet oxygen is usually monitored by a chemical method using DPBF as a probe.^[8] When reacting with singlet oxygen, DPBF converts to its endoperoxide form. Therefore the decrease of the absorbance of DPBF can be used to determine the amount of singlet oxygen. **Figure 6.6** shows the absorption spectra of ethanol solutions of DPBF and the six UCNP-RB conjugates as a function of exposure time to CW 980 nm irradiation. The main absorption band around 410 nm is due to DPBF and the 560 nm absorption band is associated with RB. The UV-Vis absorption spectrum of DPBF was taken every 5 minutes. For all samples degradation of DPBF is observed.

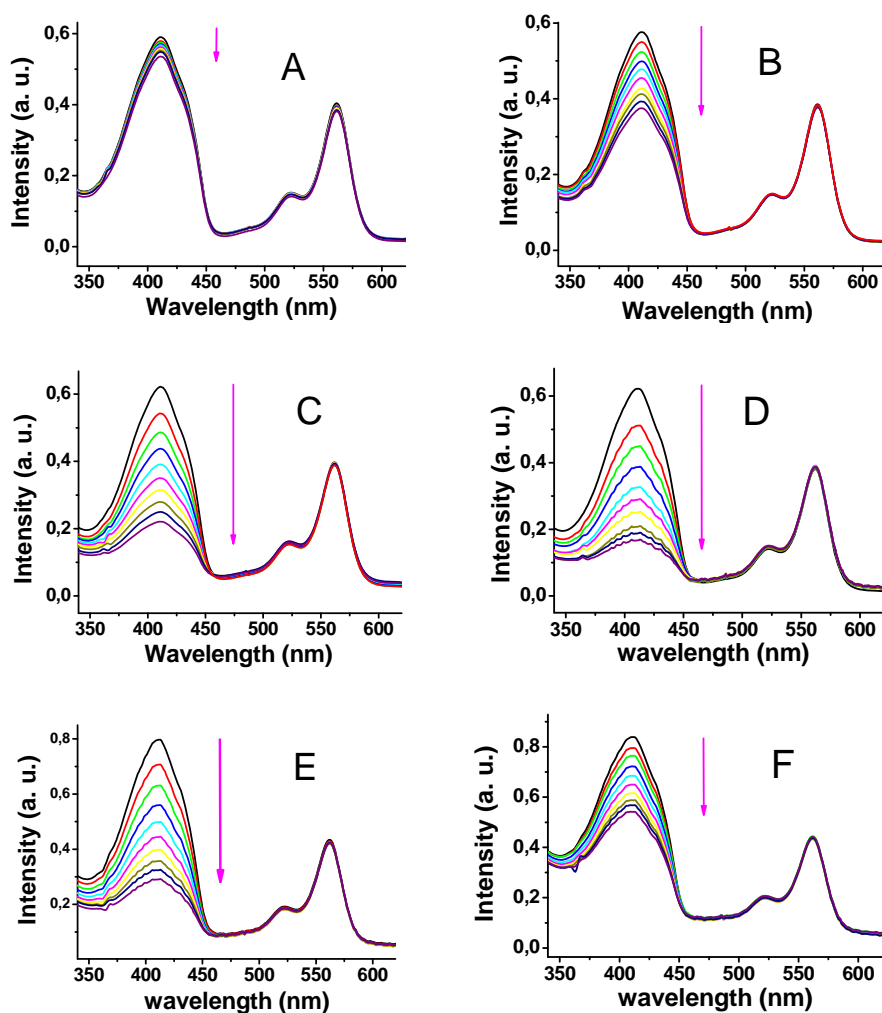


Figure 6.6. Time dependence of spectra of sample A to F under irradiation of 980 nm diode laser (730 mW). Time interval between subsequent traces is 5 minutes.

Figure 6.7 displays the absorbance of DPBF at 410 nm versus exposure time. The rate at which the curve falls off as a function of time is roughly proportional to the efficiency with which singlet oxygen is generated.^[12] It is readily seen that UCNP-RB conjugates **C**, **E**, and in particular **D** are the best in generating singlet oxygen. Thus, nanoparticles with a 16 nm core and a 6 nm shell are the best in generating $^1\text{O}_2$, although these particles show neither the strongest upconversion luminescence nor the highest energy transfer efficiency.

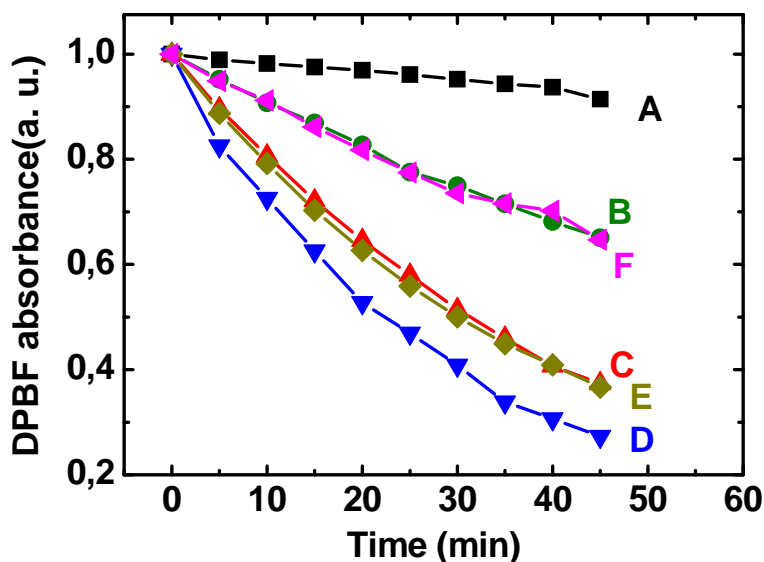


Figure 6.7. Absorbance at 410 nm of DPBF in ethanol solutions of **A** to **F** as a function of irradiation time. The excitation wavelength is at 980 nm.

6.4 Conclusions

We have studied UCNP for FRET applications with a model system of $\text{NaYF}_4:\text{Yb}^{3+}, \text{Er}^{3+}@\text{NaYF}_4$. From studies of the photophysics of UCNP-photosensitizer conjugates and studies of the generation of singlet oxygen by these conjugates we have determined the optimal shell thickness for the highest upconversion efficiency and for the FRET efficiency. Optimization of these two efficiencies requires opposing conditions: increasing the upconversion efficiency leads one to increase the shell thickness, increasing the FRET efficiency leads one to decrease the shell thickness. Since $^1\text{O}_2$ generation is determined by both processes we thus find an optimal shell thickness for $^1\text{O}_2$ generation which is a trade-off between these two conditions. In other words, our results show that to optimize UCNP based FRET conjugates one should not just be guided by only the upconversion luminescence efficiency or the FRET efficiency, but consider both at the same time.

6.5 Acknowledgments

This work was supported by an Innovation Research Program (IOP) grant of the Netherlands and by the exchange program between CAS of China and KNAW of the Netherlands, NSFC of China (60771051, 60601015, 10674132, 10874179 and 20603035).

6.6 References

- 1 (a) Fluorescence Resonant Energy Transfer Biosensor Based on Upconversion-Luminescent Nanoparticles. L. Wang, R. Yan, Z. Huo, L. Wang, J. Zeng, J. Bao, X. Wang, Q. Peng, and Y. Li; *Angew Chem. Int. Ed.*, **2005**, *44*, 6054-6057; (b) Immunoassay of Goat Antihuman Immunoglobulin G Antibody Based on Luminescence Resonance Energy Transfer between Near-Infrared Responsive NaYF₄:Yb,Er Upconversion Fluorescent Nanoparticles and Gold Nanoparticles. M. Wang, W. Hou, C.C. Mi, W.X. Wang, Z.R. Xu, H.H. Teng, C.B. Mao, and S.K. Xu; *Anal. Chem.*, **2009**, *81*, 8783 - 8789; (c) Tandem Dye Acceptor Used To Enhance Upconversion Fluorescence Resonance Energy Transfer in Homogeneous Assays. T. Rantanen, H. Pääkkilä, L. Jämsen, K. Kuningas, T. Ukonaho, T. Lövgren, and T. Soukka; *Anal. Chem.*, **2007**, *79*, 6312-6318; (d) Up-conversion FRET from Er³⁺/Yb³⁺:NaYF₄ Nanophosphor to CdSe Quantum Dots. A. Bednarkiewicz, M. Nyk, M. Samoc, and W. Stręk; *J. Phys. Chem. C*, **2010**, *114*, 17535-17541; (e) LRET-Based Biodetection of DNA Release in Live Cells Using Surface-Modified Upconverting Fluorescent Nanoparticles. H.C. Guo, N.M. Idris, and Y. Zhang; *Langmuir*, **2011**, *27*, 2854-2860; (f) Fluorescence-Quenching-Based Enzyme-Activity Assay by Using Photon Upconversion. T. Rantanen, M.L. Järvenpää, J. Vuojola, K. Kuningas, and T. Soukka; *Angew Chem. Int. Ed.*, **2008**, *47*, 3811-3813; (g) Upconversion nanoparticle-based FRET system for study of siRNA in live cells. S. Jiang and Y. Zhang; *Langmuir*, **2010**, *26*, 6689-6694; (h) Fluorescence Resonant Energy Transfer Biosensor Based on Upconversion-Luminescent Nanoparticles. L.Y. Wang, R.X. Yan, Z.Y. Huo, L. Wang, J.H. Zeng, J. Bao, X. Wang, Q. Peng, and Y.D. Li; *Angew Chem. Int. Ed.*, **2005**, *44*, 6054-6057; (i) Upconversion Fluorescence Resonance Energy Transfer in a Homogeneous Immunoassay for Estradiol. K. Kuningas, T. Ukonaho, H. Pääkkilä, T. Rantanen, J. Rosenberg, T. Lövgren, and T. Soukka; *Anal. Chem.*, **2006**, *78*, 4690-4696; (j) Versatile Synthesis Strategy for Carboxylic Acid-functionalized Upconverting Nanophosphors as Biological Labels. Z.G. Chen, H.L. Chen, H. Hu, M.X. Yu, F.Y. Li, Q. Zhang, Z.G. Zhou, T. Yi, and C.H. Huang; *J. Am. Chem. Soc.*, **2008**, *130*, 3023-3029; (k) Multicolor Core/Shell-Structured Upconversion Fluorescent Nanoparticles. Z.Q. Li, Y. Zhang, and S. Jiang; *Adv. Mater.*, **2008**, *20*, 4765-4769.
- 2 A Three-Fluorophore FRET Assay for High-Throughput Screening of Small-Molecule Inhibitors of Ribosome Assembly. D. Klostermeier, P. Sears, C.H. Wong, D.P. Millar, and J.R. Williamson; *Nucleic Acids Res.*, **2004**, *32*, 2707.
- 3 (a) FRET Imaging. E.A. Jares-Erijman, and T.M. Jovin; *Nat. Biotechnol.* **2003**, *21*, 1387-1395; (b) Introduction to Biophotonics. P.N. Prasad; *Wiley-Interscience: New York*, **2003**.

Chapter 6

- 4 (a) Semiconductor Quantum Dots for Photodynamic Therapy. A.C.S. Samia, X.B. Chen, and C. Burda; *J. Am. Chem. Soc.* **2003**, *125*, 15736; (b) Quantum dots as photosensitizers? R. Bakalova, H. Ohba, Z. Zhelev, M. Ishikawa, and Y. Baba; *Nat. Biotechnol.*, **2004**, *22*, 1360.
- 5 (a) Highly Efficient Multicolor Up-Conversion Emissions and Their Mechanisms of Monodisperse NaYF₄:Yb,Er Core and Core/Shell-Structured Nanocrystals. H.X. Mai, Y.W. Zhang, L.D. Sun, and C.H. Yan; *J. Phys. Chem. C*, **2007**, *111*, 13721-13729; (b) Water-Soluble NaYF₄:Yb,Er(Tm)/NaYF₄/Polymer Core/Shell/Shell Nanoparticles with Significant Enhancement of Upconversion Fluorescence. G.S. Yi and G.M. Chow; *Chem. Mater.*, **2007**, *19*, 341-343; (c) Synthesis, Characterization, and Spectroscopy of NaGdF₄: Ce³⁺, Tb³⁺/NaYF₄ Core/Shell Nanoparticles. J.C. Boyer, J. Gagnon, L.A. Cuccia, J.A. Capobianco; *Chem. Mater.*, **2007**, *19*, 3358-3360; (d) Synthesis and Optical Properties of KYF₄/Yb, Er Nanocrystals, and their Surface Modification with Undoped KYF₄. H. Schafer, P. Ptacek, O. Zerzouf, and M. Haase; *Adv. Funct. Mater.*, **2008**, *18*, 2913-2918; (e) Synthesis of Hexagonal-Phase Core-Shell NaYF₄ Nanocrystals with Tunable Upconversion Fluorescence. H.S. Qian and Y. Zhang; *Langmuir*, **2008**, *24*, 12123-12125; (f) Upconversion Luminescence of β -NaYF₄: Yb³⁺, Er³⁺@ β -NaYF₄ Core/Shell Nanoparticles: Excitation Power Density and Surface Dependence. Y. Wang, L.P. Tu, J.W. Zhao, Y.J. Sun, X.G. Kong, and H. Zhang; *J. Phys. Chem. C*, **2009**, *113*, 7164-7169; (g) Effect of Surface Related Organic Vibrational Modes in Luminescent Upconversion Dynamics of Rare Earth Ions Doped Nanoparticles. Y. Wang, S. Smolark, X.G. Kong, W.J. Buma, A.M. Brouwer, and H. Zhang; *J. Nanosci. Nanotechnol.*, **2010**, *10*, 7149-7153.
- 6 (a) Synthesis of Colloidal Upconverting NaYF₄ Nanocrystals Doped with Er³⁺, Yb³⁺ and Tm³⁺, Yb³⁺ via Thermal Decomposition of Lanthanide Trifluoroacetate Precursors. J.C. Boyer, F. Vetrone, L.A. Cuccia, and J.A. Capobianco; *J. Am. Chem. Soc.*, **2006**, *128*, 7444-7445; (b) Synthesis of Hexagonal-Phase NaYF₄:Yb,Er and NaYF₄:Yb,Tm Nanocrystals with Efficient Up-Conversion Fluorescence. G.S. Yi, G.M. Chow; *Adv. Funct. Mater.*, **2006**, *16*, 2324-2329.
- 7 Light-Induced Proteolysis of Myosin Heavy Chain by Rose Bengal-Conjugated Antibody Complexes. K.A. Conlon, M. Berrios; *Journal of Photochemistry and Photobiology B: Biology*, **2001**, *65*, 22-28
- 8 (a) Singlet Oxygen Quantum Yields of Different Photosensitizers in Polar Solvents and Micellar Solutions. W. Spiller, H. Kliesch, D. Wohrele, S. Hackbarth, B. Roder, and G. J. Schnurpfeil; *J. Porphyrins Phthalocyanines*, **1998**, *2*, 145; (b) Methylene Blue-Containing Silica-Coated Magnetic Particles: A Potential Magnetic Carrier for Photodynamic Therapy. D. B. Tada, L. L. R. Vono, E. L. Duarte, R. Itri, P. K. Kiyohara, M. S. Baptista, and L. M. Rossi; *Langmuir*, **2007**, *23*, 8194-8199.

-
- 9 Red Spectral Shift and Enhanced Quantum Efficiency in Phonon-Free Photoluminescence from Silicon Nanocrystals. W.D.A.M. de Boer, D. Timmerman, K. Dohnalová, I.N. Yassievich, H. Zhang, W.J. Buma, and T. Gregorkiewicz; *Nature Nanotechnology*, **2010**, 5, 878–884
- 10 Principles of Fluorescence Spectroscopy, 2nd ed.; J.R. Lakowicz; *Kluwer Academic*; New York, **1999**.
- 11 Picosecond Fluorescence Studies of Rose Bengal in Aqueous Micellar Dispersions. M.A.J. Rodgers; *Chemical Physics Letters*, **1981**, 78, 509-514.
- 12 (a) Nanomaterials and Singlet Oxygen Photosensitizers: Potential Applications in Photodynamic Therapy. S. Wang, R. Gao, F. Zhou, and M. Selke; *J. Mater. Chem.*, **2004**, 14, 487-493; (b) Organically Modified Silica Nanoparticles with Covalently Incorporated Photosensitizer for Photodynamic Therapy of Cancer. T.Y. Ohulchanskyy, I. Roy, L.N. Goswami, Y. Chen, E.J. Bergey, R.K. Pandey, A.R. Oseroff, and P.N. Prasad; *Nano. Lett.*, **2007**, 7, 2835-2842; (c) Ceramic-Based Nanoparticles Entrapping Water-Insoluble Photosensitizing Anticancer Drugs: A Novel Drug–Carrier System for Photodynamic Therapy. I. Roy, T.Y. Ohulchanskyy, H.E. Pudavar, E.J. Bergey, A.R. Oseroff, J. Morgan, T.J. Dougherty, and P.N. Prasad; *J. Am. Chem. Soc.*, **2003**, 125, 7860-7865.